Mechanically Robust All-Polymer Solar Cells from Narrow Band Gap Acceptors with Hetero-Bridging Atoms

Joule

CellPress

Article

Mechanically Robust All-Polymer Solar Cells from Narrow Band Gap Acceptors with Hetero-Bridging Atoms

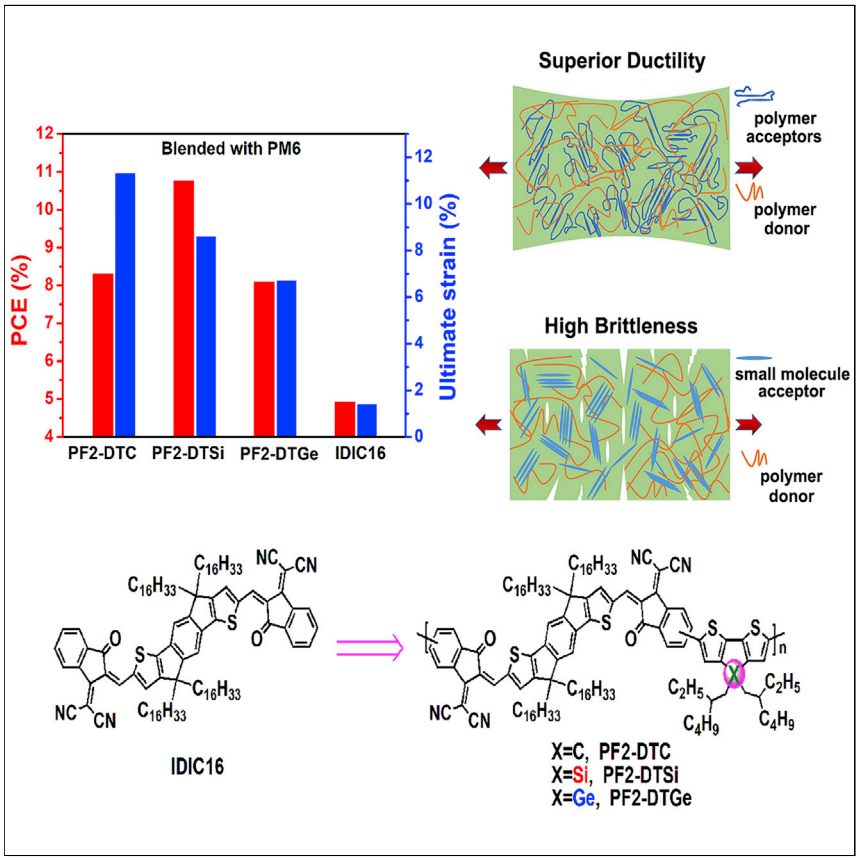

A series of polymer acceptors PF2-DTC, PF2-DTSi, and PF2-DTGe with identical molecular backbone but different central bridging atoms in tricyclic-fused donor units were developed. In all-PSCs, the PF2-DTSi-based blend film exhibited excellent mechanical robustness with an impressively high PCE of up to 10.77%. Moreover, the flexible solar cell based on this blend retained >90% of its initial PCE after bending and relaxing 1,200 times at a bending radius of ~4 mm.

Qunping Fan, Wenyan Su, Shanshan Chen, ..., He Yan, Donghong Yu, Ergang Wang

tskim1@kaist.ac.kr (T.-S.K.)
thlt@jnu.edu.cn (L.H.)
yang@unist.ac.kr (C.Y.)
ergang@chalmers.se (E.W.)

HIGHLIGHTS

Polymer acceptors with different bridging atoms (C, Si, and Ge) were synthesized

Si-bridged PF2-DTSi achieved a PCE of up to 10.77% in all-PSCs

The PF2-DTSi-based flexible all-PSCs have excellent mechanical robustness

Fan et al., Joule 4, 658–672
March 18, 2020
https://doi.org/10.1016/j.joule.2020.01.014

Joule

CellPress

Article

Mechanically Robust All-Polymer Solar Cells from Narrow Band Gap Acceptors with Hetero-Bridging Atoms

Qunping Fan,[1,14] Wenyan Su,[1,2,14] Shanshan Chen,[3,7,14] Wansun Kim,[5] Xiaobin Chen,[6] Byongkyu Lee,[3] Tao Liu,[8] Ulises A. Méndez-Romero,[1,13] Ruijie Ma,[8] Tao Yang,[4] Wenliu Zhuang,[9] Yu Li,[9] Yaowen Li,[6] Taek-Soo Kim,[5,*] Lintao Hou,[2,*] Changduk Yang,[3,*] He Yan,[8] Donghong Yu,[10,11] and Ergang Wang[1,12,15,*]

SUMMARY

We developed three narrow band-gap polymer acceptors PF2-DTC, PF2-DTSi, and PF2-DTGe with different bridging atoms (i.e., C, Si, and Ge). Studies found that such different bridging atoms significantly affect the crystallinity, extinction coefficient, electron mobility of the polymer acceptors, and the morphology and mechanical robustness of related active layers. In all-polymer solar cells (all-PSCs), these polymer acceptors achieved high power conversion efficiencies (PCEs) over 8.0%, while PF2-DTSi obtained the highest PCE of 10.77% due to its improved exciton dissociation, charge transport, and optimized morphology. Moreover, the PF2-DTSi-based active layer showed excellent mechanical robustness with a high toughness value of 9.3 MJ m^{-3} and a large elongation at a break of 8.6%, which is a great advantage for the practical applications of flexible devices. As a result, the PF2-DTSi-based flexible all-PSC retained >90% of its initial PCE (6.37%) after bending and relaxing 1,200 times at a bending radius of ~4 mm.

INTRODUCTION

Just within the last five years, tremendous advances in nonfullerene acceptors (NFAs), including both small molecules (SMs)[1–7] and polymers,[8–14] have greatly improved the photovoltaic (PV) performance of polymer solar cells (PSCs). Power conversion efficiencies (PCEs) exceeding 16% have been achieved in their PV devices.[15–20] Compared to the SM-acceptor-based PSCs, all-polymer solar cells (all-PSCs) based on an active layer consisting of one polymer acceptor and one polymer donor with excellent morphological stability and mechanical robustness,[21–23] are considered to be the most promising candidates for PV devices. However, compared to the diversity of most popular SM-NFAs,[1–7] the types and quantities of polymer acceptors are scarce and structurally limited to such few units as perylene diimide (PDI),[8,24] naphthalene diimide (NDI),[9,25] and B→N-bridged bipyridine building blocks.[10] Until now, the most widely used polymer acceptor is the NDI-based narrow band-gap N2200,[9] and its relevant all-PSCs have achieved a high PCE over 8% from different research groups by using various optically complementary polymer donors.[26–29] However, N2200 film displays a very low extinction coefficient of ~0.3 × 10^5 cm^{-1}, which seriously limits the further improvement of short-circuit current density (J_{sc}) and PCE in its all-PSCs. Recently, Zhang and Li et al. reported an important alternative narrow band-gap polymer acceptor PZ1

Context & Scale

All-polymer solar cells have unique advantages of excellent morphological stability and mechanical robustness and are considered to have great practical application prospects. Studies have shown that bridging atoms can fine-tune the photoelectric properties of photovoltaic materials. However, there have been no reports on how bridging atoms of polymer acceptors effect on the molecular characters and active layer morphologies so far. Herein, polymer acceptors with different bridging atoms (C, Si, and Ge) were developed, and it was found that bridging atoms significantly affect the molecular absorption and electron mobility, as well as the morphology and mechanical robustness of active layers. As a result, the active layer based on Si-bridged PF2-DTSi shows excellent mechanical robustness and the related rigid and flexible all-PSCs achieved the PCEs of 10.77% and 6.37%, respectively. This work provides a useful strategy to develop efficient polymer acceptors by optimizing bridging atoms for all-PSCs.

with a high absorption coefficient (~1.3×10^5 cm^{-1}) by embedding a large π-fused acceptor-donor-acceptor (A-D-A)-structured building block (IDIC16) into the polymer backbone, and the related all-PSCs achieved an impressive PCE up to 9.19% and a high J_{sc} of 16.05 mA cm^{-2}.[11] Subsequently, by screening the donor units, another polymer acceptor PFBDT-IDTIC based on IDIC16 building block was synthesized by Yan et al. and obtained a high PCE over 10% in its all-PSCs.[30] Although great progress has been made in all-PSCs recently, their device efficiencies are still lower than the requirement of practical applications, which is mainly attributed to the limited number of candidates for high-performance polymer acceptors. Moreover, it is noticed that the study of mechanical properties of active layers from all-PSCs is almost confined to the NDI-based polymer acceptors.[31,32] So far, the mechanical properties of the active layers based on polymer acceptors with a building block of IDIC or ITIC derivatives have never been studied.

In the active layers of all-PSCs, excessive interchain entanglement often exists between polymers, which leads to poor morphology of active layers.[33] To improve the device efficiency of all-PSCs, various approaches for controlling and optimizing the active layer morphology have been explored successfully in various degrees, such as solvent and solid additives,[34] third component,[35] and solvent and/or thermal annealing.[36] In terms of molecular design, ternary copolymerization strategy of polymer acceptors can optimize the related active layer morphologies by optimizing molecular crystallinity.[37–39] Moreover, recent studies have shown that molecular side-chain engineering[40] and halogenation[41] can also improve the photoelectric properties of polymer acceptors. However, the above strategies are almost confined to the design of NDI- or PDI-type polymer acceptors with a low extinction coefficient so far, which hinders the further improvements on PCEs of all-PSCs. Therefore, developing an effective molecular design strategy to construct high-performance polymer acceptors with excellent photophysical and electrochemical properties and optimizing the active layer morphologies is one of the long-term challenges in the progress of efficient all-PSCs.

Some recent studies have shown that bridging atoms can fine-tune the photoelectric properties of the SM-donors and polymer donors and the related morphological behavior, resulting in improved PCEs in photovoltaic devices.[42–44] On the other hand, up to now, there have been no reports on the effects of bridging atoms with different atomic sizes, mass densities, and bond lengths on the molecular characters, crystallinity, and the related active layer morphologies of polymer acceptors bearing the same backbone. Herein, we firstly designed and synthesized a series of narrow band-gap polymer acceptors (PF2-DTC, PF2-DTSi, and PF2-DTGe) that consist of the same IDIC16 building block as acceptor unit and different central bridging atoms-fused tricyclic donor units, as shown in Scheme 1. Our studies find that bridging atoms rarely change the absorption spectra or energy levels but significantly affect the extinction coefficient, crystallinity, and electron mobility of polymer acceptors. Moreover, the morphology, molecular order, and mechanical robustness of related active layers are also obviously affected by these different bridging atoms. Matched with a medium band-gap polymer donor PM6[45–47] in PV devices, all-PSCs achieved much higher PCEs of >8% compared to their contrast SM-acceptor IDIC16-based PSCs (4.93%), while PF2-DTSi obtained the highest PCE of up to 10.77% due to its improved photoelectric properties and active layer morphology. Moreover, studies have shown that the active layers containing these polymer acceptors have much better mechanical robustness than the IDIC16-based contrast blends, which is of great advantage for the practical applications of flexible devices in future. As a result, the PF2-DTSi-based flexible all-PSC achieved a high PCE of 6.37% and

[1]Department of Chemistry and Chemical Engineering, Chalmers University of Technology, Göteborg, SE-412 96, Sweden

[2]Guangdong Provincial Key Laboratory of Optical Fiber Sensing and Communications, Guangzhou Key Laboratory of Vacuum Coating Technologies and New Energy Materials, Siyuan Laboratory, Department of Physics, Jinan University, Guangzhou 510632, China

[3]Department of Energy Engineering, School of Energy and Chemical Engineering, Low Dimensional Carbon Materials Center, Ulsan National Institute of Science and Technology (UNIST), Ulsan 44919, South Korea

[4]TEMA-NRG, Mechanical Engineering Department, University of Aveiro, 3810-193 Aveiro, Portugal

[5]Department of Mechanical Engineering, Korea Advanced Institute of Science and Technology (KAIST), Daejeon 34141, South Korea

[6]Laboratory of Advanced Optoelectronic Materials, College of Chemistry, Chemical Engineering and Materials Science, Soochow University, Suzhou 215123, China

[7]MOE Key Laboratory of Low-grade Energy Utilization Technologies and Systems, CQU-NUS Renewable Energy Materials & Devices Joint Laboratory, School of Energy & Power Engineering, Chongqing University, Chongqing 400044, China

[8]Department of Chemistry and Hong Kong Branch of Chinese National Engineering Research Center for Tissue Restoration & Reconstruction, Hong Kong University of Science and Technology, Clear Water Bay, Kowloon, 999077, Hong Kong

[9]Advanced Research Center for Polymer Processing Engineering of Guangdong Province, Guangdong Research Center for Special Building Materials and Its Green Preparation Technology, Guangdong Industry Polytechnic, Guangzhou 510300, China

[10]Department of Chemistry and Bioscience, Aalborg University, DK-9220, Aalborg, Denmark

[11]Sino-Danish Center for Education and Research, Aarhus, DK-8000, Denmark

[12]School of Materials Science and Engineering, Zhengzhou University, Zhengzhou 450001, China

[13]Centro de Investigación en Materiales Avanzados S.C. (CIMAV), Unidad Monterrey, Apodaca 66628, Mexico

[14]These authors contributed equally to this work

[15]Lead Contact

*Correspondence: tskim1@kaist.ac.kr (T.-S.K.), thlt@jnu.edu.cn (L.H.), yang@unist.ac.kr (C.Y.), ergang@chalmers.se (E.W.)

https://doi.org/10.1016/j.joule.2020.01.014

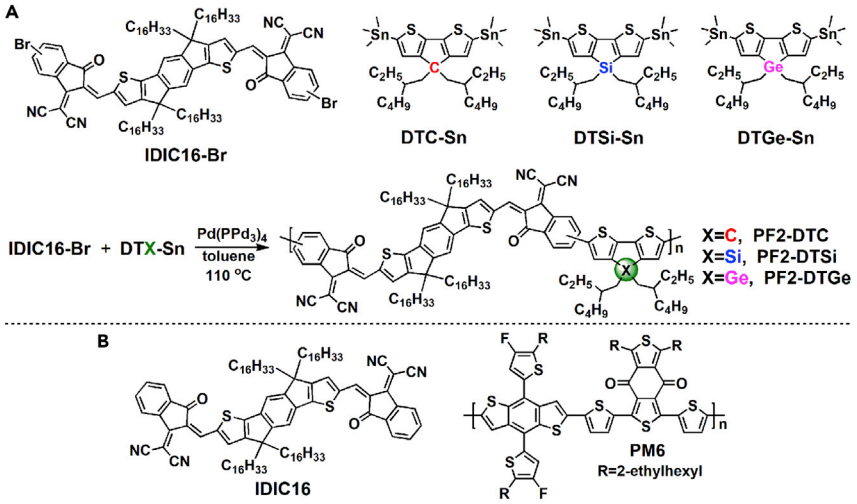

Scheme 1. Chemical Information of the Donor and Acceptors

(A) Synthetic routes and molecular structures of three polymer acceptors PF2-DTC, PF2-DTSi, and PF2-DTGe.

(B) Molecular structures of SM-acceptor IDIC16 and polymer donor PM6.

retained >90% of its initial PCE after bending and relaxing up to 1,200 times at a bending radius of ~4 mm. Our results provide an effective strategy to develop high-performance polymer acceptors by optimizing bridging atoms in the fused cyclic donor moieties for efficient all-PSCs.

RESULTS AND DISCUSSION

Three polymer acceptors were synthesized by Stille-coupling polymerization, and the corresponding number-averaged molecular weight and polydispersity index were determined as 23.8 kDa and 3.92 for PF2-DTC, 27.0 kDa and 2.70 for PF2-DTSi, and 21.8 kDa and 2.42 for PF2-DTGe, respectively. Due to the long alkyl side chains in both acceptor and donor units, these polymer acceptors show reasonably high molecular weights but still good solubility in common organic solvents such as toluene, chlorobenzene, and chloroform.

The absorption spectra of active layer materials in films are plotted in Figure 1A. All polymer acceptors show almost identical absorption spectra (normalized), with the related absorption onset and optical gap being ~785 nm and ~1.57 eV, respectively. Compared with SM-acceptor IDIC16, polymer acceptors show more than 50 nm red-shifted absorption ranges, which could complement the absorption of the polymer donor PM6 in a better manner. As shown in Figure S1, the PM6:polymer acceptor blend films show a wide absorption range of 300~785 nm. Although the central bridging atoms in tricyclic-fused donor units have little effects on the absorption ranges of polymer acceptors in this case, they result in slightly different extinction coefficients (Figure S2), in which PF2-DTSi film shows the highest one. The results show that our optimization of central bridging atoms in tricyclic-fused donor units can effectively improve their optical absorption.

The energy levels of active layer materials are summarized in Figure 1B. All polymer acceptors show comparable lowest unoccupied molecular orbital (LUMO) levels of −3.87 ~ −3.90 eV, which are close to that of SM-acceptor IDIC16 (−3.88 eV), but slightly upshifted HOMO levels, leading to narrower band gap. Since the three

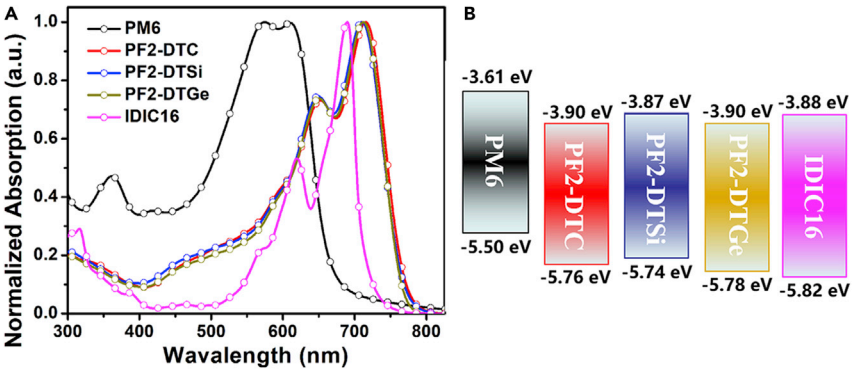

Figure 1. Optical Absorption and Energy Levels of the Donor and Acceptors

(A) Normalized absorption spectra of polymer donor PM6, polymer acceptors PF2-DTC, PF2-DTSi, PF2-DTGe, and SM-acceptor IDIC16 in films.

(B) Molecular energy level diagrams of polymer donor PM6, polymer acceptors PF2-DTC, PF2-DTSi, PF2-DTGe, and SM-acceptor IDIC16 in films.

polymer acceptors have almost the same LUMO levels and clearly red-shifted absorption spectra compared to their structural analog SM-acceptor IDIC16, our polymerization strategy is expected to develop high-performance polymer acceptors with high J_{sc} values without sacrificing open-circuit voltage (V_{oc}) in devices.

As shown in Figure 4, from the grazing incidence wide-angle X-ray scattering (GIWAXS) measurements, all of the three polymer acceptor films show a predominant "face-on" orientation with a lamellar (100) diffraction peak at ~0.25 $Å^{-1}$ in their in-plane (IP) profiles and a strong π-π stacking (010) diffraction peak at ~1.60 $Å^{-1}$ in their out-of-plane (OOP) profiles. The corresponding crystallite coherence lengths (CCL) can be calculated, whereas PF2-DTSi film shows slightly increased π-face-on CCL_{010} value of 14.77 Å as compared to PF2-DTC (14.37 Å) and PF2-DTGe (14.31 Å) films. As shown in Figure S3A, PF2-DTSi has a higher electron mobility (μ_e) of 2.98 × 10^{-4} cm^2 V^{-1} s^{-1} compared to PF2-DTC (1.19 × 10^{-4} cm^2 V^{-1} s^{-1}) and PF2-DTGe (0.85 × 10^{-4} cm^2 V^{-1} s^{-1}) estimated by the space charge limited current (SCLC) method. It is interesting to note that even the SM-acceptor IDIC16 presents several arc-like multiple peaks with a greater CCL_{010} value of up to 51.68 Å, the μ_e of SM-acceptor IDIC16 was only 1.28 × 10^{-4} cm^2 V^{-1} s^{-1}, which is lower than that of PF2-DTSi neat film. This is probably due to the fact that the charge transport along the conjugated polymer chains is more efficient than that along π-π stacking direction.[48]

To probe the effect of central bridging atoms in tricyclic-fused donor units on the photovoltaic performance of these polymer acceptors, all-PSCs with a device structure of ITO/PEDOT:PSS/PM6:PF2-DTX/PFN-Br/Al were fabricated. All the all-PSCs underwent the same process optimization because of their structural similarities, in which the active layers with an optimized thickness of ~110 nm were obtained from a spin-coated binary blend solution of chloroform:chloronaphthalene (*v/v*, 100:6) with a D/A ratio (*w/w*) of 2:1 and a total solid concentration of 10 mg mL^{-1}. As a representative, the detailed optimization processes and photovoltaic parameters of the PM6:PF2-DTSi-based active layer are summarized in Figures S4 and S5; Tables S1 and S2. The current density-voltage (*J-V*) curves and related device data of the optimized all-PSCs based on different polymer acceptors, as well as the PSCs based on SM-acceptor IDIC16 as a contrast are displayed in Figure 2A and Table 1. Compared to the IDIC16-based PSCs with a PCE less than 5%, the all-PSCs achieved much higher PCEs of over 8%, which are attributed to the significantly increased J_{sc} and fill factor (FF) without sacrificing V_{oc}. Moreover, the

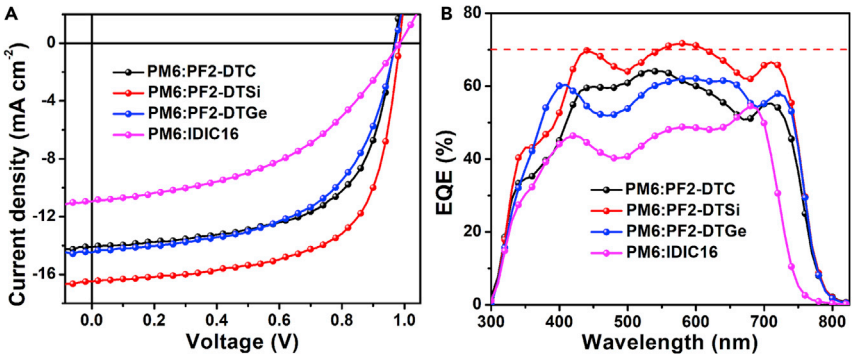

Figure 2. Photovoltaic Properties of the PM6-Based PSCs with Different Acceptors

(A) The *J-V* plots of the optimized PV devices based on polymer acceptors and SM-acceptor under the illumination of AM 1.5G, 100 mW cm^{-2}.

(B) The corresponding EQE spectra of PV devices.

PM6:PF2-DTSi-based all-PSCs achieved an impressively high PCE of up to 10.77% with a slightly increased V_{oc} of 0.99 V, and significantly improved J_{sc} of 16.48 mA cm^{-2} and FF of 0.661 in comparison with the all-PSCs based on PM6:PF2-DTC (PCE = 8.31%, V_{oc} = 0.97 V, J_{sc} = 14.11 mA cm^{-2}, and FF = 0.608) and PM6:PF2-DTGe (PCE = 8.09%, $V_{o\,c}$ = 0.97 V, J_{sc} = 14.48 mA cm^{-2}, and FF = 0.576). The remarkably high PV performance of PF2-DTSi among the all-PSCs indicates the clear benefit of our design strategy by introducing Si-heteroatom as the central bridge of tricyclic-fused donor unit into the polymer backbone. A structural analog to PF2-DTSi bearing the same acceptor unit but a dramatically different donor moiety (one thiophene unit), namely PZ1, had resulted in PCE of 9.19% and 11.2% when blending with PBDB-T and PM6, respectively.[11,49] In order to investigate the effect of different electron push-pull strength between PF2-DTSi and PZ1 on their PV performance, the PM6:PZ1-based all-PSC was fabricated under the same conditions and achieved a slightly lower PCE of 10.4% compared to the PM6:PF2-DTSi-based ones, as shown in Figure S6. Moreover, the small molecule with shorter side chains named IDIC was also used as acceptor for comparison in this work. The PM6:IDIC-based PSC delivered a PCE of 11.1% (close to the reported value of 11.9%[47]), comparable to that from the PM6:PF2-DTSi-based all-PSCs but much higher than that from PM6:IDIC16-based one (shown in Figure S7). This indicates the alkyl chains have an essential influence on the PV performance of the resulting materials. However, the attempt to synthesize PF2-DTSi with shorter side chains (containing IDIC units) leads to insoluble polymer.

As shown in Figure 2B, the J_{sc} values of devices were verified by the external quantum efficiency (EQE) measurements. Compared to the IDIC16-based PSC, the all-PSCs display obviously red-shifted EQE spectra range and higher EQE values. Moreover, the PF2-DTSi-based device shows higher EQE response in a wide spectrum range of 400∼750 nm compared to the PF2-DTC and PF2-DTGe-based devices, which is consistent with its higher absorption coefficient. As a result, the PM6:PF2-DTSi-based all-PSCs achieved the highest EQE value of more than 70%. The mismatches between the calculated J_{sc} from integrating EQEs with solar radiation spectrum and the measured J_{sc} from J-V plots for the three all-PSCs are less than 5%, indicating the reliability of the device data.

To further understand the reasons for why the PM6:PF2-DTSi-based all-PSCs have higher photovoltaic performance than the other devices, the exciton dissociation probability $P(E,T)$, recombination mechanism, photoluminescence (PL)-quenching

Table 1. Photovoltaic Parameters of the Optimized PV Devices Based on Polymer Acceptors and SM-Acceptor under the Illumination of AM 1.5G, 100 mW cm^{-2}

D:A	V_{oc} [V]	J_{sc} [mA cm^{-2}]	FF	PCE [%]
PM6:PF2-DTC	0.97	14.11 (13.88)[a]	0.608	8.31 (8.12)[b]
PM6:PF2-DTSi	0.99	16.48 (16.07)[a]	0.661	10.77 (10.63)[b]
PM6:PF2-DTGe	0.97	14.48 (14.16)[a]	0.576	8.09 (7.89)[b]
PM6:IDIC16	0.98	10.96 (10.42)[a]	0.457	4.93 (4.64)[b]

[a]The integrated J_{sc} (in parenthesis) from the EQE curves with solar radiation spectrum.
[b]The average PCEs (in parenthesis) calculated from 15 devices.

efficiencies, and charge mobilities of the active layers and related devices were investigated. The $P(E,T)$ values were estimated by the plots of photocurrent (J_{ph}) versus effective voltage (V_{eff}) from devices.[50,51] As shown in Figure 3A and Table 2, the devices based on polymer acceptors show significantly increased $P(E,T)$ of 71.1%∼76.3% compared to that based on SM-acceptor (51.6%) under the maximal power output conditions. Moreover, the all-PSC based on PF2-DTSi exhibits higher $P(E,T)$ value of 76.3% in comparison with those all-PSC based on PF2-DTC (73.4%) and PF2-DTGe (71.1%), indicating appropriate contributions on the optimized exciton dissociation and charge extraction properties of the related devices by introducing tricyclic-fused donor units with different central bridging atoms into the polymer backbone.

The charge recombination of devices can be studied by investigating the effect of light irradiation intensity (P) on the J_{sc} (i.e., $J_{sc} \propto P^S$) and V_{oc}, respectively. As shown in Figure 3B, compared with the SM-acceptor IDIC16-based PSCs with a S value of 0.928, the all-PSCs display higher ones of 0.960∼0.965 that are close to 1. This clearly demonstrates decreased bimolecular recombination for each related device by introducing such hetero-tricyclic-fused donor units into polymer backbones.[50,52] As shown in Figure 3C, among the three all-PSCs, PM6:PF2-DTSi shows the smallest slope (1.16 kT/q), being the closest to 1 kT/q (where k, T, and q are the Boltzmann constant, Kelvin temperature, and elementary charge, respectively) in all devices,[50,53] which reveals limited trap-assisted recombination of the related devices by the modification of central bridging atom in tricyclic-fused donor units. Moreover, as shown in Figure S3 and Table 2, the PM6:PF2-DTSi blends show higher and more balanced hole- and electron-mobilities of 1.47×10^{-4} and 3.27×10^{-4} cm^2 V^{-1} s^{-1} in device compared to the PM6:PF2-DTC (1.03×10^{-4} and 2.95×10^{-4} cm^2 V^{-1} s^{-1}) and PM6:PF2-DTGe (0.99×10^{-4} and 1.74×10^{-4} cm^2 V^{-1} s^{-1}), which is conducive to suppressing the accumulation of space charge in related all-PSCs.

The PL spectra of the PM6 pure film and related blend films with different acceptors are shown in Figure 3D. Compared to the emission of the film of neat PM6, films of all the polymer acceptors-based blends claimed high PL-quenching efficiencies over 90%, while the IDIC16-based blends exhibited a low one below 85%. Moreover, among the three all-polymer acceptor-based blend films, PM6:PF2-DTSi blend film achieved the highest PL-quenching efficiency up to 95.6%, indicating the most efficient photo-induced charge transfer from PM6 to PF2-DTSi, which may be due to its good morphological compatibilities. Similarly, as seen in Figure S8, efficient charge transfer also occurs from all three polymer acceptors and SM-acceptor IDIC16 to donor polymer PM6 when comparing the emission between their neat films and their blends with PM6. All-polymers blend films again show higher PL-quenching efficiencies in comparison with the PM6:IDIC16 blend film, while PM6:PF2-DTSi blend film still displays the highest PL-quenching efficiency.

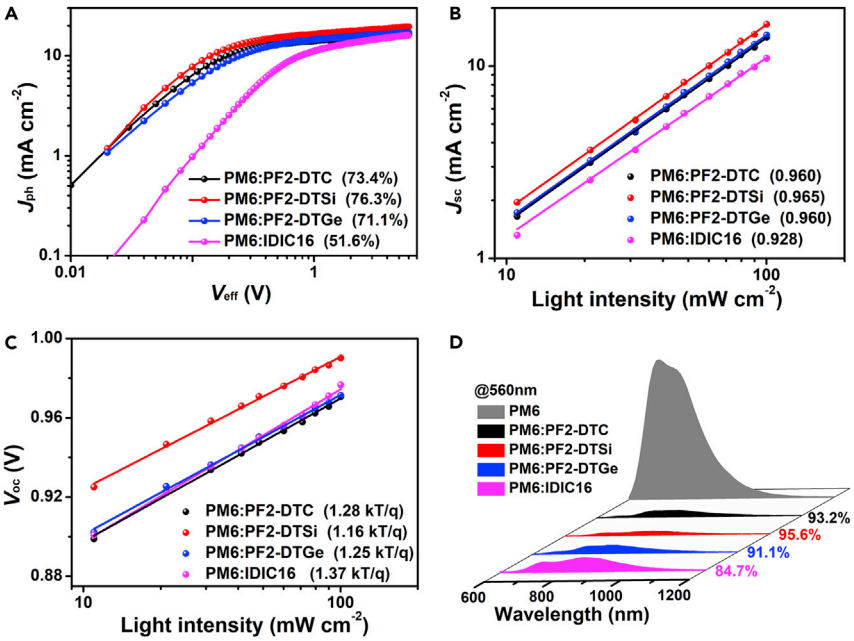

Figure 3. The Characteristics of Charge Dynamic in the PM6-Based PSCs with Different Acceptors

(A) The J_{ph} versus V_{eff} of the PM6-based PSCs with different acceptors.

(B) The J_{sc} versus light intensity of the PM6-based PSCs with different acceptors.

(C) The V_{oc} versus light intensity of the PM6-based PSCs with different acceptors.

(D) The PL spectra of PM6 pure film and the related blend films with different acceptors.

The molecular crystallinity and packing of the blend films were also probed by the GIWAXS measurements. Figure 4A shows the 2D GIWAXS diffraction patterns of the blend films, and the related OOP and IP line-cuts are summarized in Figures 4B and 4C. All the three all-polymer blend films exhibit a mixture of "edge-on" and "face-on" orientations. Such 3-D textures are known to facilitate the co-existence of both parallel and vertical charge transport pathways in the active layers, contributing effective charge transport process in the devices.[54] In IP direction, these all-polymer blend films show obvious (100) diffraction peaks at a similar position of ~0.29 Å^{-1}. The PM6:PF2-DTC and PM6:PF2-DTSi blend films show much higher CCL_{100} values of 145.0~150.6 Å than that of 126.1 Å for the PM6:PF2-DTGe blend, while the PM6:PF2-DTSi blend film has the highest CCL_{100} of 150.6 Å. As shown in Figure S9, the pole figure analysis extracted from the alkyl side chains (100) reflection of blend films was executed to get deeper insight into their structural orientation. The related areas integrated with polar angle χ ranges of −45° to 45° (A_z), −90° to −45°, and 45° to 90° (A_{xy}) belong to the fractions of π-edge-on and π-face-on domains, respectively.[55] Therefore, their ratios can be calculated by A_{xy}/A_z. Such calculated A_{xy}/A_z value is 1.224 for the PM6:PF2-DTSi blend film, indicating a greater proportion of π-face-on domains versus π-edge-on ones, whereas the PM6:PF2-DTC (A_{xy}/A_z = 0.901) and PM6:PF2-DTGe (A_{xy}/A_z = 0.905) blend films show the primarily oriented π-edge-on. Because the donor polymer is highly disordered, the paracrystallinity g-factor analysis of the blend films was also carried out to estimate the degree of crystallinity using the (100) alkyl stacking diffraction peak in IP directions. According to previous reports,[56,57] the blend film has amorphous texture if the related g-factor is larger than 10%. The g-factor is 14.36% for the PM6:PF2-DTSi blend film, which is smaller than the other two blend films of PM6:PF2-DTC (14.53%) and PM6:PF2-DTGe (15.63%). Therefore, among the

Table 2. Data Summaries of the PM6-Based PSCs with Different Acceptors

Active Layers	$P(E,T)$	S Value	Slope Value	μ_h [$cm^2\ V^{-1}\ s^{-1}$]	μ_e [$cm^2\ V^{-1}\ s^{-1}$]	μ_h/μ_e
PM6:PF2-DTC	73.4%[a]	0.960[b]	1.28 kT/q[c]	1.03×10^{-4}	2.95×10^{-4}	0.35
PM6:PF2-DTSi	76.3%[a]	0.965[b]	1.16 kT/q[c]	1.47×10^{-4}	3.27×10^{-4}	0.45
PM6:PF2-DTGe	71.1%[a]	0.960[b]	1.25 kT/q[c]	0.99×10^{-4}	1.74×10^{-4}	0.57
PM6:IDIC16	51.6%[a]	0.928[b]	1.37 kT/q[c]	0.81×10^{-4}	0.46×10^{-4}	1.76

[a]From the curves of J_{ph} versus V_{eff} of PSCs.
[b]From the curves of J_{sc} versus light intensity of PSCs.
[c]From the curves of V_{oc} versus light intensity of PSCs.

all-polymer blend films, the PM6:PF2-DTSi blend film could be regarded as the closest to partially paracrystalline.

Compared to the polymer acceptor neat films, the all-polymer blend films show an additional (200) peak at ~0.65 $Å^{-1}$ in IP directions, which is contributed by the polymer donor PM6. Moreover, the all-polymer blend films display significantly sharper (100) peaks in IP directions compared to their polymer acceptor neat films, which is attributed to the improved crystallization via the use of CN additives in blend films. In other reports,[11,30,49,58] with the use of CN as additives, the all-polymer blend films based on the polymer acceptors with long alkyl chains also showed similar phenomena with sharper (100) peaks and enhanced crystallinities, which may be due to the longer crystallization time of long alkyl chain. Moreover, the PM6:PF2-DTSi shows an obviously stronger (010) peak in the OOP direction compared to the PM6:PF2-DTC and PM6:PF2-DTGe. Upon mixing with polymer donor PM6, the π-face-on CCL_{010} values of all-polymer blends are significantly enhanced and show a gradual increment in the order of PM6:PF2-DTGe (19.01 Å) < PM6:PF2-DTC (21.32 Å) < PM6:PF2-DTSi (21.35 Å), which is consistent with the trend observed in polymer acceptor neat films. The improved size of crystallites and molecular packing of the PM6:PF2-DTSi blending system are expected to help refraining the trap-assisted recombination and improve the charge transport process for achieving high J_{sc} and FF in all-PSCs.[59–61] On the other hand, for the PM6:IDIC16 blends, overlapping double (010) diffractions in OOP direction induced by each component in blends, are clearly observed. The corresponding π-face-on CCL_{010} values are 72.55 and 28.87 Å for the PM6 and IDIC16 in blend films, respectively, much higher than that of neat films, suggesting the excessive self-aggregation in this system.

The morphologies of active layers also were investigated by atomic force microscopy (AFM) and transmission electron microscopy (TEM) measurements. As shown in Figures 5A–5C, all-polymer acceptor-based blend films in the height images exhibit smoother surface morphologies with a smaller root-mean-square roughness (R_q) of 2.42~3.17 nm compared to IDIC16-based blend film (4.79 nm). Moreover, with the increase of the atomic mass of the central bridging atoms in tricyclic-fused donor units of polymer acceptors, the related blend films show a gradual decrease in surface roughness, which is consistent to the decreasing domain size of blend films in phase images (Figures 5E–5G). As shown in Figures 5I–5L, the TEM images of the all-polymer blend films exhibit more distinct fibril texture compared to the PM6:IDIC16-based blend film. The suitable surface roughness and phase separation of all-polymer blend films are in good agreement with the higher photovoltaic performance of the related all-PSCs. Moreover, among the all-polymer blend films, the PM6:PF2-DTSi blend film shows the moderate surface roughness (Figure 5B) and phase separation (Figures 5F and 5J), which is conducive to suppress the charge

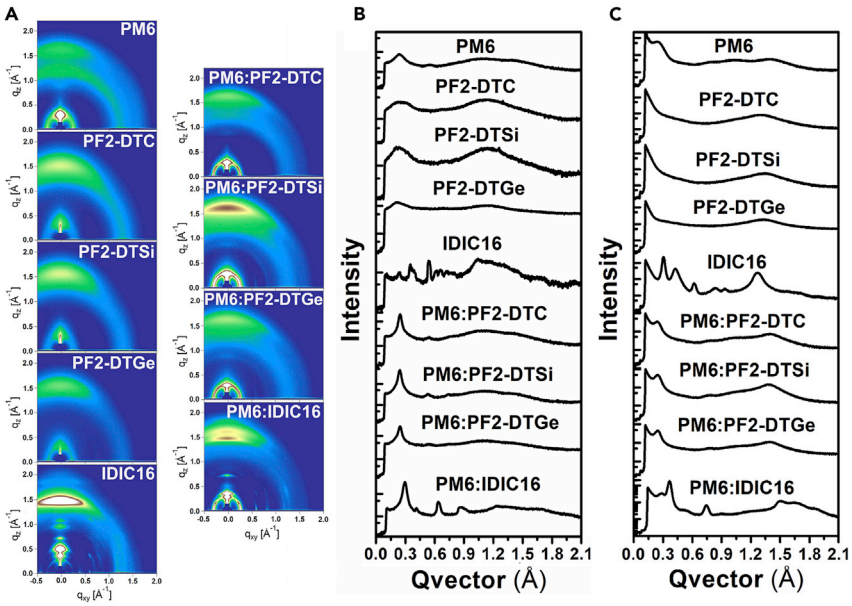

Figure 4. 2D Profiles and the Related Line-Cuts of the GIWAXS Patterns of the Pure Films and Related Blend Films

(A) The 2D GIWAXS profiles of the pure films and related blend films.

(B) The related IP line-cuts from the pure films and related blend films.

(C) The related OOP line-cuts from the pure films and related blend films.

recombination and improve the photocurrent generation in efficient all-PSCs. This can also support the best PV performance obtained from this blend.

The roll-to-roll (R2R) process for the fabrication of large-area photovoltaic devices requires flexible substrates with good stretchable property, therefore, it is important that active layer has good mechanical robustness that can bear it. Moreover, the previous studies from Krebs et al. showed that improving the mechanical integrity of the flexible and wearable photovoltaic devices to ensure the long-term stability is a priority for commercialization.[62] For example, the PSCs as wearable electronics should have a tensile strain over 20%, which occurs by delicate muscle movements of human body activity.[63] However, the study of mechanical properties of active layer in PSCs have been very limited, especially a direct comparison of the mechanical behaviors between the active layers based on structurally similar but different acceptor types (such as SM-acceptor and related SM-based polymer acceptor) has not been investigated. To evaluate the potential practical applications of the three polymer acceptors in R2R process and wearable electronics, the mechanical robustness of the polymer acceptor neat films (Figure S10 and Table S3) and the related all-polymer active layers (Figure 6 and Table 3) was studied by employing a pseudo free-standing tensile test system (Figures S11 and S12).[64] As shown in Figure S10 and Table S3, with the increase of the bridging atom mass in polymer acceptors, their neat films show rapidly decreasing elongation at break (from 31.7% to 14.6%, and then to 5.9%), tensile strength (from 24.9 to 20.5, and then to 17.5 MPa), and elastic modulus (from 1.06 to 0.93, and then to 0.67 GPa) in turn. As a result, the related polymer acceptor neat films achieve rapidly decreasing integrated toughness from 6.61 to 2.50, and then to 0.83 MJ m^{-3} in turn, which indicates that the increase of bridging atom mass reduces the mechanical properties of related polymer acceptors.

As shown in Figure 6A of the representative stress-strain plots, compared to the PM6:SM-acceptor active layer exhibiting a poor mechanical robustness with an

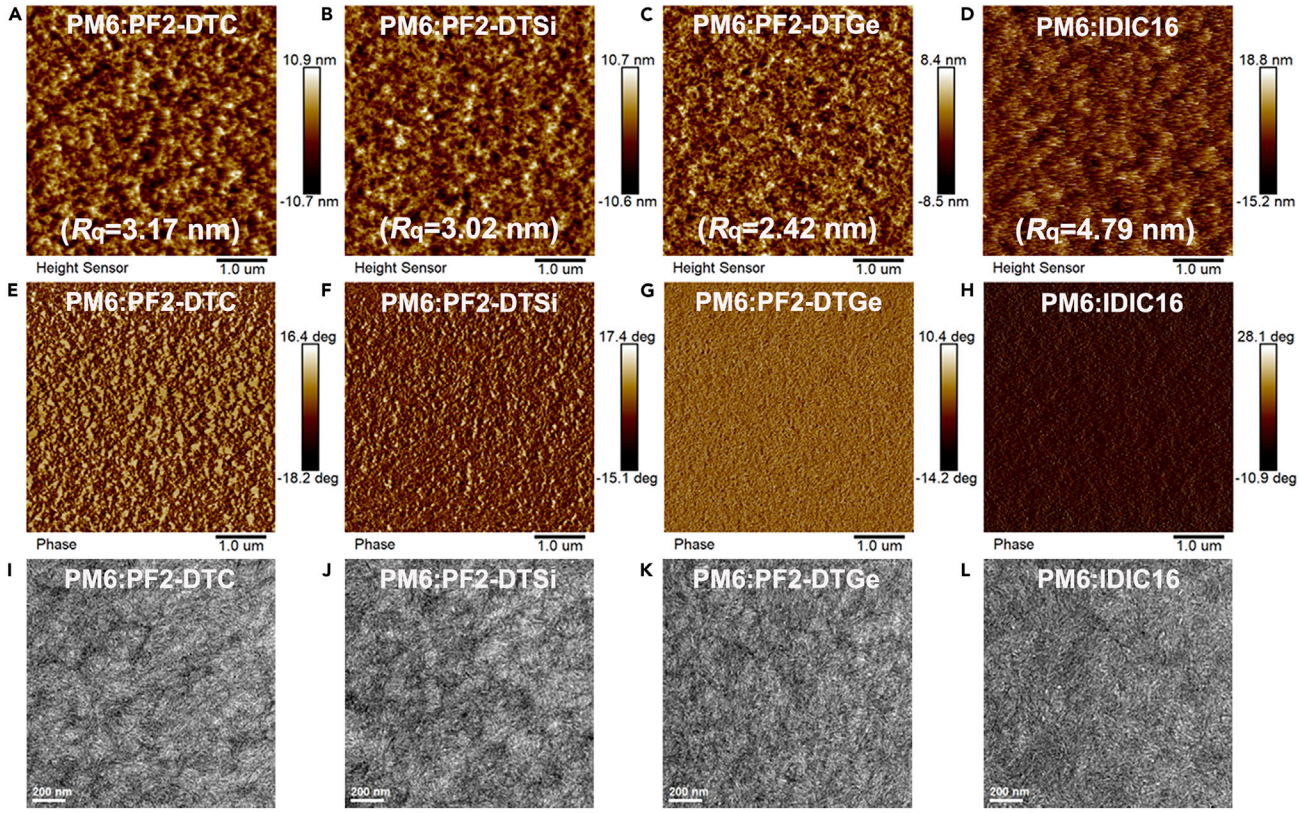

Figure 5. The Height (Top Row) and Phase (Middle Row) AFM Images and TEM Images (Bottom Row) of the Blend Films

(A), (E), and (I) for PM6:PF2-DTC blend film.

(B), (F), and (J) for PM6:PF2-DTSi blend film.

(C), (G), and (K) for PM6:PF2-DTGe blend film.

(D), (H), and (L) for PM6:IDIC16 blend film.

obviously brittle fracture even at a very low strain of ~1.4%, all the all-polymer active layers display distinct plastic deformation regions and higher mechanical robustness. As shown in Figure 6B, the all-polymer active layers have excellent elongation at break of 6.7%~11.3%, which is 5~8 fold higher compared to that of the PM6:SM-acceptor active layer. From PM6:PF2-DTC to PM6:PF2-DTSi and then to PM6:PF2-DTGe, the related active layers show decreasing elongation at break in turn, which is consistent with the strain properties of their polymer acceptor neat films. Among the all-polymer active layers, the PM6:PF2-DTSi active layer shows a medium elongation at break of 8.6% $\pm$ 1.6%, which well meets the R2R process for fabrication of large area photovoltaic devices and the practical application of wearable electronics when combined with flexible substrates.[31,65] Moreover, as shown in Figure 6C, all of the all-polymer active layers show significantly increased tensile strength of 15.5~17.3 MPa in comparison with the PM6:IDIC16 active layer (10.4 MPa). One of the reasons for the poor elongation at break and tensile strength of the PM6:IDIC16 active layer may be that the strong crystallinity of IDIC16 in blend system (see Figure 4) leads to large brittleness. As shown in Figure 6D, compared to the PM6:IDIC16 active layer with an elastic modulus of 1.03 GPa, the all-polymer active layers show the decreased elastic modulus of 0.72~0.99 GPa, indicating that the rigidity and stiffness of the active layer in PSCs can be significantly decreased by our polymerization strategy. Moreover, the PM6:PF2-DTSi active layer shows a lower elastic modulus of 0.72 GPa than those of 0.99 and 0.79 GPa for the

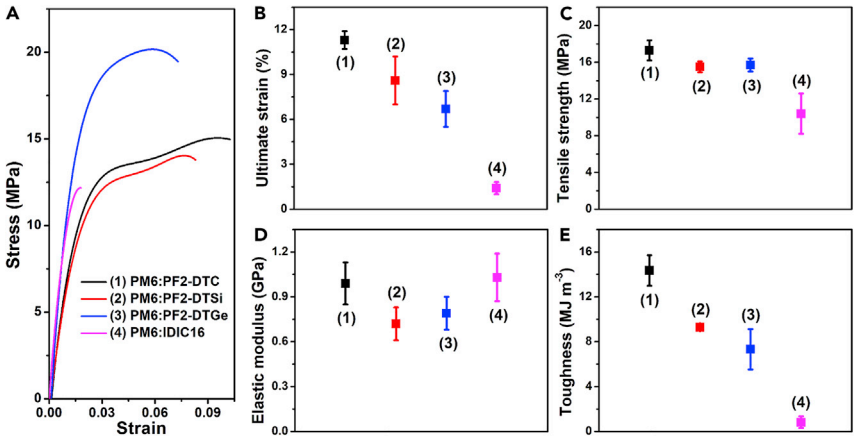

Figure 6. The Mechanical Robustness Properties of the Active Layers under a Pseudo Free-Standing Tensile Test System and the Related Statistical Values from Five Specimens

(A) The strain-stress curves of active layers.

(B) The statistical values of ultimate strain of active layers.

(C) The statistical values of tensile strength of active layers.

(D) The statistical values of elastic modulus of active layers.

(E) The statistical values of toughness of active layers.

active layers based on PM6:PF2-DTC and PM6:PF2-DTGe, respectively, indicating that the rigidity and stiffness of the active layer in PSCs can be further decreased by hetero bridging atom engineering. As a result, the all-polymer active layers achieve much higher integrated toughness values of 7.33∼14.35 MJ m^{-3}, which is 9∼18 fold higher compared to the PM6:SM-acceptor active layer (0.82 MJ m^{-3}), as shown in Figure 6E.

Since the all-polymer blend films have much better mechanical properties than the PM6:IDIC16 blend film, their flexible devices were also fabricated for comparison. As shown in Figure S13 and Table S4, the PM6:PF2-DTSi-based flexible all-PSC shows a distinctly higher PCE of 6.37% than that of 2.70% from the PM6:IDIC16-based ones. As shown in Figure S14, the PM6:PF2-DTSi-based flexible all-PSC retains >90% of its initial PCE after bending and relaxing from up to 1,200 times at a bending radius of ∼4 mm, which is much better than the PM6:IDIC16-based PSC keeping only ∼75% of its initial PCE. From this important and interesting measurement, we can further conclude that good mechanical property of active layers can significantly contribute to the mechanical stability of the device. This important finding further highlights the great advantages of all-PSCs and their bright future for practical applications using R2R process.[66] Moreover, it is worth noting that these all-polymer blend films achieved decent mechanical robustness (Figure S15 and Table S5) but much higher performance in photovoltaic devices compared to other reported works, especially the PM6:PF2-DTSi blends with a high PCE of 10.77% in all-PSCs and a moderate elongation at break of 8.6%. It has to be noticed that this is the first direct comparison of mechanical robustness between structurally similar polymer:SM (PM6:IDIC16) and polymer:polymer (PM6:IDIC16-based polymer) active layer films. The mechanical robustness of the classical polymer acceptor N2200 and related PM6:N2200 blends was also measured for comparison. As shown in Figure S16 and Table S6, compared to the PF2-DTSi neat film, the N2200 neat film shows a similar elongation at break of 14.6% but significantly lower tensile strength of 12.8 MPa, as well as a much lower tensile toughness of 1.62 MJ m^{-3}. Compared to the PM6:PF2-DTSi blends, the PM6:N2200 blends has a higher elongation at break of

Table 3. Mechanical Parameters of the Blend Films from Five Specimens

Blend Films	Ultimate Strain [%]	Tensile Strength [MPa]	Elastic Modulus [GPa]	Toughness [MJ m^{-3}]
PM6:PF2-DTC	11.3 ± 0.6	17.3 ± 1.1	0.99 ± 0.14	14.35 ± 1.36
PM6:PF2-DTSi	8.6 ± 1.6	15.5 ± 0.6	0.72 ± 0.11	9.30 ± 0.09
PM6:PF2-DTGe	6.7 ± 1.2	15.7 ± 0.7	0.79 ± 0.11	7.33 ± 1.80
PM6:IDIC16	1.4 ± 0.4	10.4 ± 2.2	1.03 ± 0.16	0.82 ± 0.52

13.4%, a similar tensile strength of 15.2 MPa but a large elastic modulus of 0.84 GPa, resulting in an obviously lower integrated toughness of 1.68 MJ m^{-3}. Considering that the PM6:PF2-DTSi-based all-PSC has a higher PCE compared to PM6:N2200-based all-PSCs with a PCE of 5.97% (Figure S17), the PM6:PF2-DTSi-based all-PSCs have higher practical application prospects in the future. This result clearly demonstrated the advantages of the PM6:PF2-DTSi-based all-PSCs with both high PCE in device and excellent mechanical robustness for practical R2R processing and wearable electronics in the future.

In conclusion, a series of narrow band-gap polymer acceptors PF2-DTC, PF2-DTSi, and PF2-DTGe with identical molecular backbone but different central bridging atoms in tricyclic-fused donor units were developed. Our studies show that central bridging atoms hardly influence the optical absorption and LUMO levels but significantly affect the crystallinity and charge mobility properties of polymer acceptors, as well as the morphology, molecular order, and mechanical robustness of the resulting active layers. Matched with polymer donor PM6, these all-PSCs achieved PCEs over 8%, while the PF2-DTSi-based all-PSCs got an impressively high PCE of up to 10.77% due to the improved exciton dissociation and charge transport, less charge recombination, higher PL-quenching efficiency, and optimized active layer morphology than C and Ge bridged ones. More importantly, it was found that the active layers containing polymer acceptors have excellent and higher mechanical robustness compared to the blends based on the contrast SM-acceptor IDIC16, which is of great advantage for the practical R2R process and applications of flexible devices in the future. As a result, the PM6:PF2-DTSi-based flexible all-PSC achieved a high PCE of 6.37% and retained >90% of its initial PCE after bending and relaxing up to 1,200 times at a bending radius of ~4 mm. Our results provide an effective way to develop high-performance polymer acceptors by optimizing central bridging atoms for efficient and mechanically robust all-PSCs.

EXPERIMENTAL PROCEDURES

Full experimental procedures are provided in the Supplemental Information.

SUPPLEMENTAL INFORMATION

Supplemental Information can be found online at https://doi.org/10.1016/j.joule.2020.01.014.

ACKNOWLEDGMENTS

We thank the Swedish Research Council, the Swedish Research Council Formas, the Wallenberg Foundation (2017.0186 and 2016.0059) for financial support. We also appreciate support from NSFC project (61774077), Guangzhou Municipal Science and Technology Bureau (201804010501), Department of Education of Guangdong Province (2018GKTSCX041, 2017GKCXTD001, and 2017GKQNCX005), Guangdong Province Higher Vocational Colleges and Schools Pearl River Scholar Funded

Scheme (2015 and 2018), Guangzhou Science and Technology Plan (201804010295 and 201904010381), and the China Scholarship Council (201908440047). Yaowen Li thanks the financial support from Collaborative Innovation Center of Suzhou Nano Science and Technology and Collaborative Innovation Center for New-type Urbanization and Social Governance of Jiangsu Province. D.Y. thanks the financial support from Innovation fund Denmark (INKA project) and Sino-Danish Centre for Education and Research (SDC). This work was supported by Wearable Platform Materials Technology Center (WMC, no. 2016R1A5A1009926) funded by the National Research Foundation of Korea (NRF) Grant by the Korean Government (MSIT).

AUTHOR CONTRIBUTIONS

Q.F. and E.W. conceived the idea. Q.F. and U.A.M.R. synthesized the polymers. W.S., Q.F., and L.H. discussed, fabricated, and optimized the PSCs devices. S.C., B.L., and C.Y. characterized the GIWAXS. W.K. and T.S.K. measured the pseudo free-standing tensile test. X.C. and Yaowen Li fabricated the flexible PSCs. Q.F., W.S., T.L., R.M., and T.Y. contributed to material and device characterization. Q.F., E.W., W.Z., Y.L., H.Y., and D.Y. drafted the manuscript with input from all co-authors. E.W. supervised and directed the project.

DECLARATION OF INTERESTS

The authors declare no competing interests.

Received: October 15, 2019
Revised: December 14, 2019
Accepted: January 21, 2020
Published: February 17, 2020

REFERENCES

1. Lin, Y., Wang, J., Zhang, Z.G., Bai, H., Li, Y., Zhu, D., and Zhan, X. (2015). An electron acceptor challenging fullerenes for efficient polymer solar cells. Adv. Mater. *27*, 1170–1174.

2. Zhao, W., Li, S., Yao, H., Zhang, S., Zhang, Y., Yang, B., and Hou, J. (2017). Molecular optimization enables over 13% efficiency in organic solar cells. J. Am. Chem. Soc. *139*, 7148–7151.

3. Huang, H., Guo, Q., Feng, S., Zhang, C., Bi, Z., Xue, W., Yang, J., Song, J., Li, C., Xu, X., et al. (2019). Noncovalently fused-ring electron acceptors with near-infrared absorption for high-performance organic solar cells. Nat. Commun. *10*, 3038.

4. Du, X., Heumueller, T., Gruber, W., Classen, A., Unruh, T., Li, N., and Brabec, C.J. (2019). Efficient polymer solar cells based on non-fullerene acceptors with potential device lifetime approaching 10 years. Joule *3*, 215–226.

5. Yuan, J., Zhang, Y., Zhou, L., Zhang, G., Yip, H.-L., Lau, T.-K., Lu, X., Zhu, C., Peng, H., Johnson, P.A., et al. (2019). Single-junction organic solar cell with over 15% efficiency using fused-ring acceptor with electron-deficient core. Joule *3*, 1140–1151.

6. Meng, L., Zhang, Y., Wan, X., Li, C., Zhang, X., Wang, Y., Ke, X., Xiao, Z., Ding, L., Xia, R., et al. (2018). Organic and solution-processed tandem solar cells with 17.3% efficiency. Science *361*, 1094–1098.

7. Baran, D., Ashraf, R.S., Hanifi, D.A., Abdelsamie, M., Gasparini, N., Röhr, J.A., Holliday, S., Wadsworth, A., Lockett, S., Neophytou, M., et al. (2017). Reducing the efficiency-stability-cost gap of organic photovoltaics with highly efficient and stable small molecule acceptor ternary solar cells. Nat. Mater. *16*, 363–369.

8. Zhan, X., Tan, Z.A., Domercq, B., An, Z., Zhang, X., Barlow, S., Li, Y., Zhu, D., Kippelen, B., and Marder, S.R. (2007). A high-mobility electron-transport polymer with broad absorption and its use in field-effect transistors and all-polymer solar cells. J. Am. Chem. Soc. *129*, 7246–7247.

9. Yan, H., Chen, Z., Zheng, Y., Newman, C., Quinn, J.R., Dötz, F., Kastler, M., and Facchetti, A. (2009). A high-mobility electron-transporting polymer for printed transistors. Nature *457*, 679–686.

10. Long, X., Ding, Z., Dou, C., Zhang, J., Liu, J., and Wang, L. (2016). Polymer acceptor based on double B←N bridged bipyridine (BNBP) unit for high-efficiency all-polymer solar cells. Adv. Mater. *28*, 6504–6508.

11. Zhang, Z.G., Yang, Y., Yao, J., Xue, L., Chen, S., Li, X., Morrison, W., Yang, C., and Li, Y. (2017). Constructing a strongly absorbing low-bandgap polymer acceptor for high-performance all-polymer solar cells. Angew. Chem. Int. Ed. Engl. *56*, 13503–13507.

12. Guo, Y., Li, Y., Awartani, O., Han, H., Zhao, J., Ade, H., Yan, H., and Zhao, D. (2017). Improved performance of all-polymer solar cells enabled by naphthodiperylenetetraimide-based polymer acceptor. Adv. Mater. *29*, 28467000.

13. Zhou, E., Nakano, M., Izawa, S., Cong, J., Osaka, I., Takimiya, K., and Tajima, K. (2014). All-polymer solar cell with high near-infrared response based on a naphthodithiophene diimide (NDTI) copolymer. ACS Macro Lett. *3*, 872–875.

14. Zhou, N., Dudnik, A.S., Li, T.I., Manley, E.F., Aldrich, T.J., Guo, P., Liao, H.C., Chen, Z., Chen, L.X., Chang, R.P.H., et al. (2016). All-polymer solar cell performance optimized via systematic molecular weight tuning of both donor and acceptor polymers. J. Am. Chem. Soc. *138*, 1240–1251.

15. Cui, Y., Yao, H., Zhang, J., Zhang, T., Wang, Y., Hong, L., Xian, K., Xu, B., Zhang, S., Peng, J., et al. (2019). Over 16% efficiency organic photovoltaic cells enabled by a chlorinated acceptor with increased open-circuit voltages. Nat. Commun. *10*, 2515.

16. Li, K., Wu, Y., Tang, Y., Pan, M.A., Ma, W., Fu, H., Zhan, C., and Yao, J. (2019). Ternary blended fullerene-free polymer solar cells with 16.5% efficiency enabled with a higher-LUMO-

level acceptor to improve film morphology. Adv. Energy Mater. *9*, 1901728.

17. An, Q., Ma, X., Gao, J., and Zhang, F. (2019). Solvent additive-free ternary polymer solar cells with 16.27% efficiency. Science Bulletin *64*, 504–506.

18. Ma, Y., Zhou, X., Cai, D., Tu, Q., Ma, W., and Zheng, Q. (2020). A minimal benzo[c][1,2,5] thiadiazole-based electron acceptor as a third component material for ternary polymer solar cells with efficiencies exceeding 16.0%. Materials Horizons *7*, 117–124.

19. Hong, L., Yao, H., Wu, Z., Cui, Y., Zhang, T., Xu, Y., Yu, R., Liao, Q., Gao, B., Xian, K., et al. (2019). Eco-compatible solvent-processed organic photovoltaic cells with over 16% efficiency. Adv. Mater. *31*, e1903441.

20. Fan, B., Zhang, D., Li, M., Zhong, W., Zeng, Z., Ying, L., Huang, F., and Cao, Y. (2019). Achieving over 16% efficiency for single-junction organic solar cells. Sci. China Chem. *62*, 746–752.

21. Wang, G., Melkonyan, F.S., Facchetti, A., and Marks, T.J. (2019). All-polymer solar cells: recent progress, challenges, and prospects. Angew. Chem. Int. Ed. Engl. *58*, 4129–4142.

22. Su, W., Fan, Q., Guo, X., Guo, B., Li, W., Zhang, Y., Zhang, M., and Li, Y. (2016). Efficient ternary blend all-polymer solar cells with a polythiophene derivative as a hole-cascade material. J. Mater. Chem. A *4*, 14752–14760.

23. Genene, Z., Mammo, W., Wang, E., and Andersson, M.R. (2019). Recent advances in n-type polymers for all-polymer solar cells. Adv. Mater *31*, e1807275.

24. Zhou, Y., Kurosawa, T., Ma, W., Guo, Y., Fang, L., Vandewal, K., Diao, Y., Wang, C., Yan, Q., Reinspach, J., et al. (2014). High performance all-polymer solar cell via polymer side-chain engineering. Adv. Mater *26*, 3767–3772.

25. Kolhe, N.B., Tran, D.K., Lee, H., Kuzuhara, D., Yoshimoto, N., Koganezawa, T., and Jenekhe, S.A. (2019). New random copolymer acceptors enable additive-free processing of 10.1% efficient all-polymer solar cells with near-unity internal quantum efficiency. ACS Energy Lett. *4*, 1162–1170.

26. Fan, B., Zhong, W., Ying, L., Zhang, D., Li, M., Lin, Y., Xia, R., Liu, F., Yip, H.L., Li, N., et al. (2019). Surpassing the 10% efficiency milestone for 1-cm^2 all-polymer solar cells. Nat. Commun. *10*, 4100.

27. Zhu, L., Zhong, W., Qiu, C., Lyu, B., Zhou, Z., Zhang, M., Song, J., Xu, J., Wang, J., Ali, J., et al. (2019). Aggregation-induced multilength scaled morphology enabling 11.76% efficiency in all-polymer solar cells using printing fabrication. Adv. Mater *31*, e1902899.

28. Xu, Y., Yuan, J., Zhou, S., Seifrid, M., Ying, L., Li, B., Huang, F., Bazan, G.C., and Ma, W. (2019). Ambient processable and stable all-polymer organic solar cells. Adv. Funct. Mater. *29*, 1806747.

29. Gao, L., Zhang, Z.G., Xue, L., Min, J., Zhang, J., Wei, Z., and Li, Y. (2016). All-polymer solar cells based on absorption-complementary polymer donor and acceptor with high power conversion efficiency of 8.27%. Adv. Mater *28*, 1884–1890.

30. Yao, H., Bai, F., Hu, H., Arunagiri, L., Zhang, J., Chen, Y., Yu, H., Chen, S., Liu, T., Lai, J.Y.L., et al. (2019). Efficient all-polymer solar cells based on a new polymer acceptor achieving 10.3% power conversion efficiency. ACS Energy Lett. *4*, 417–422.

31. Kim, T., Kim, J.H., Kang, T.E., Lee, C., Kang, H., Shin, M., Wang, C., Ma, B., Jeong, U., Kim, T.S., and Kim, B.J. (2015). Flexible, highly efficient all-polymer solar cells. Nat. Commun *6*, 8547.

32. Choi, J., Kim, W., Kim, S., Kim, T.S., and Kim, B.J. (2019). Influence of acceptor type and polymer molecular weight on the mechanical properties of polymer solar cells. Chem. Mater *31*, 9057–9069.

33. Lee, C., Lee, S., Kim, G.U., Lee, W., and Kim, B.J. (2019). Recent advances, design guidelines, and prospects of all-polymer solar cells. Chem. Rev. *119*, 8028–8086.

34. Liu, X., Zhang, C., Duan, C., Li, M., Hu, Z., Wang, J., Liu, F., Li, N., Brabec, C.J., Janssen, R.A.J., et al. (2018). Morphology optimization via side chain engineering enables all-polymer solar cells with excellent fill factor and stability. J. Am. Chem. Soc. *140*, 8934–8943.

35. Benten, H., Nishida, T., Mori, D., Xu, H., Ohkita, H., and Ito, S. (2016). High-performance ternary blend all-polymer solar cells with complementary absorption bands from visible to near-infrared wavelengths. Energy Environ. Sci. *9*, 135–140.

36. Li, Z., Xu, X., Zhang, W., Meng, X., Ma, W., Yartsev, A., Inganäs, O., Andersson, M.R., Janssen, R.A.J., and Wang, E. (2016). High performance all-polymer solar cells by synergistic effects of fine-tuned crystallinity and solvent annealing. J. Am. Chem. Soc. *138*, 10935–10944.

37. Chen, D., Yao, J., Chen, L., Yin, J., Lv, R., Huang, B., Liu, S., Zhang, Z.G., Yang, C., Chen, Y., and Li, Y. (2018). Dye-incorporated polynaphthalenediimide acceptor for additive-free high-performance all-polymer solar cells. Angew. Chem. Int. Ed. Engl. *57*, 4580–4584.

38. Dang, D., Yu, D., and Wang, E. (2019). Conjugated donor-acceptor terpolymers toward high-efficiency polymer solar cells. Adv. Mater *31*, e1807019.

39. Hwang, Y.J., Earmme, T., Courtright, B.A., Eberle, F.N., and Jenekhe, S.A. (2015). n-type semiconducting naphthalene diimide-perylene diimide copolymers: controlling crystallinity, blend morphology, and compatibility toward high-performance all-polymer solar cells. J. Am. Chem. Soc. *137*, 4424–4434.

40. Liu, S., Kan, Z., Thomas, S., Cruciani, F., Brédas, J.L., and Beaujuge, P.M. (2016). Thieno[3,4-c] pyrrole-4,6-dione-3,4-difluorothiophene polymer acceptors for efficient all-polymer bulk heterojunction solar cells. Angew. Chem. Int. Ed. Engl. *55*, 12996–13000.

41. Sun, H., Tang, Y., Koh, C.W., Ling, S., Wang, R., Yang, K., Yu, J., Shi, Y., Wang, Y., Woo, H.Y., and Guo, X. (2019). High-performance all-polymer solar cells enabled by an n-type polymer based on a fluorinated imide-functionalized arene. Adv. Mater. *31*, e1807220.

42. Wang, E., Wang, L., Lan, L., Luo, C., Zhuang, W., Peng, J., and Cao, Y. (2008). High-performance polymer heterojunction solar cells of a polysilafluorene derivative. Appl. Phys. Lett. *92*, 23.

43. Eisenmenger, N.D., Su, G.M., Welch, G.C., Takacs, C.J., Bazan, G.C., Kramer, E.J., and Chabinyc, M.L. (2013). Effect of bridging atom identity on the morphological behavior of solution-processed small molecule bulk heterojunction photovoltaics. Chem. Mater *25*, 1688–1698.

44. Amb, C.M., Chen, S., Graham, K.R., Subbiah, J., Small, C.E., So, F., and Reynolds, J.R. (2011). Dithienogermole as a fused electron donor in bulk heterojunction solar cells. J. Am. Chem. Soc. *133*, 10062–10065.

45. Zhang, M., Guo, X., Ma, W., Ade, H., and Hou, J. (2015). A large-bandgap conjugated polymer for versatile photovoltaic applications with high performance. Adv. Mater. *27*, 4655–4660.

46. Fan, Q., Su, W., Wang, Y., Guo, B., Jiang, Y., Guo, X., Liu, F., Russell, T.P., Zhang, M., and Li, Y. (2018). Synergistic effect of fluorination on both donor and acceptor materials for high performance non-fullerene polymer solar cells with 13.5% efficiency. Sci. China Chem. *61*, 531–537.

47. Fan, Q., Wang, Y., Zhang, M., Wu, B., Guo, X., Jiang, Y., Li, W., Guo, B., Ye, C., Su, W., et al. (2018). High-performance as-cast nonfullerene polymer solar cells with thicker active layer and large area exceeding 11% power conversion efficiency. Adv. Mater. *30*, 1704546.

48. Li, W., Wang, D., Wang, S., Ma, W., Hedström, S., James, D.I., Xu, X., Persson, P., Fabiano, S., Berggren, M., et al. (2015). One-step synthesis of precursor oligomers for organic photovoltaics: a comparative study between polymers and small molecules. ACS Appl. Mater. Interfaces *7*, 27106–27114.

49. Meng, Y., Wu, J., Guo, X., Su, W., Zhu, L., Fang, J., Zhang, Z., Liu, F., Zhang, M., Russell, T.P., and Li, Y. (2019). 11.2% Efficiency all-polymer solar cells with high open-circuit voltage. Sci. China Chem. *62*, 845–850.

50. Blom, P.W., Mihailetchi, V., Koster, L.J.A., and Markov, D.E. (2007). Device physics of polymer: fullerene bulk heterojunction solar cells. Adv. Mater *19*, 1551–1566.

51. Zhou, Z., Xu, S., Song, J., Jin, Y., Yue, Q., Qian, Y., Liu, F., Zhang, F., and Zhu, X. (2018). High-efficiency small-molecule ternary solar cells with a hierarchical morphology enabled by synergizing fullerene and non-fullerene acceptors. Nat. Energy *3*, 952–959.

52. Chen, H., Hu, Z., Wang, H., Liu, L., Chao, P., Qu, J., Chen, W., Liu, A., and He, F. (2018). A chlorinated π-conjugated polymer donor for efficient organic solar cells. Joule *2*, 1623–1634.

53. Li, S., Zhan, L., Sun, C., Zhu, H., Zhou, G., Yang, W., Shi, M., Li, C.Z., Hou, J., Li, Y., and Chen, H. (2019). Highly efficient fullerene-free organic solar cells operate at near zero highest occupied molecular orbital offsets. J. Am. Chem. Soc. *141*, 3073–3082.

54. Chen, S., Lee, S.M., Xu, J., Lee, J., Lee, K.C., Hou, T., Yang, Y., Jeong, M., Lee, B., Cho, Y., et al. (2018). Ultrafast channel II process

induced by a 3-D texture with enhanced acceptor order ranges for high-performance non-fullerene polymer solar cells. Energy Environ. Sci. *11*, 2569–2580.

55. Vohra, V., Kawashima, K., Kakara, T., Koganezawa, T., Osaka, I., Takimiya, K., and Murata, H. (2015). Efficient inverted polymer solar cells employing favourable molecular orientation. Nat. Photonics *9*, 403–408.

56. Wang, G., Swick, S.M., Matta, M., Mukherjee, S., Strzalka, J.W., Logsdon, J.L., Fabiano, S., Huang, W., Aldrich, T.J., Yang, T., et al. (2019). Photovoltaic blend microstructure for high efficiency post-fullerene solar cells. To tilt or not to tilt? J. Am. Chem. Soc. *141*, 13410–13420.

57. Rivnay, J., Noriega, R., Northrup, J.E., Kline, R.J., Toney, M.F., and Salleo, A. (2011). Structural origin of gap states in semicrystalline polymers and the implications for charge transport. Phys. Rev. B *83*, 121306.

58. Wu, J., Meng, Y., Guo, X., Zhu, L., Liu, F., and Zhang, M. (2019). All-polymer solar cells based on a novel narrow-bandgap polymer acceptor with power conversion efficiency over 10%. J. Mater. Chem. A *7*, 16190–16196.

59. Fan, Q., Xu, Z., Guo, X., Meng, X., Li, W., Su, W., Ou, X., Ma, W., Zhang, M., and Li, Y. (2017). High-performance nonfullerene polymer solar cells with open-circuit voltage over 1 V and energy loss as low as 0.54 eV. Nano Energy *40*, 20–26.

60. An, Q., Zhang, F., Gao, W., Sun, Q., Zhang, M., Yang, C., and Zhang, J. (2018). High-efficiency and air stable fullerene-free ternary organic solar cells. Nano Energy *45*, 177–183.

61. Liu, T., Luo, Z., Fan, Q., Zhang, G., Zhang, L., Gao, W., Guo, X., Ma, W., Zhang, M., Yang, C., et al. (2018). Use of two structurally similar small molecular acceptors enabling ternary organic solar cells with high efficiencies and fill factors. Energy Environ. Sci. *11*, 3275–3282.

62. Jørgensen, M., Norrman, K., Gevorgyan, S.A., Tromholt, T., Andreasen, B., and Krebs, F.C. (2012). Stability of polymer solar cells. Adv. Mater *24*, 580–612.

63. Mun, J., Wang, G.N., Oh, J.Y., Katsumata, T., Lee, F.L., Kang, J., Wu, H.C., Lissel, F., Rondeau-Gagné, S., Tok, J.B.-H., et al. (2018). Effect of nonconjugated spacers on mechanical properties of semiconducting polymers for stretchable transistors. Adv. Funct. Mater *28*, 1804222.

64. Chen, S., Jung, S., Cho, H.J., Kim, N.H., Jung, S., Xu, J., Oh, J., Cho, Y., Kim, H., Lee, B., et al. (2018). Highly flexible and efficient all-polymer solar cells with high-viscosity processing polymer additive toward potential of stretchable devices. Angew. Chem. Int. Ed. Engl. *57*, 13277–13282.

65. O'Connor, T.F., Zaretski, A.V., Shiravi, B.A., Savagatrup, S., Printz, A.D., Diaz, M.I., and Lipomi, D.J. (2014). Stretching and conformal bonding of organic solar cells to hemispherical surfaces. Energy Environ. Sci. *7*, 370–378.

66. Li, Y., Xu, G., Cui, C., and Li, Y. (2018). Flexible and semitransparent organic solar cells. Adv. Energy Mater. *8*, 1701791.